ELSEVIER

Fluid Dynamics Research 16 (1995) 275–295

FLUID DYNAMICS RESEARCH

The random sweeping decorrelation hypothesis in stratified turbulent flows

Gabriel Katul[a], Marc Parlange[b], John Albertson[b], Chia-Ren Chu[c]

[a]*School of the Environment, Duke University, Durham, NC 27708-0328, USA*
[b]*Hydrologic Science, University of California, Davis, CA 95616, USA*
[c]*Department of Civil Engineering, National Central University, Chung-Li, Taiwan*

Received 12 September 1994

Longitudinal velocity measurements above a uniform dry lakebed were carried out to investigate the applicability of the random sweeping decorrelation hypothesis to thermally stratified turbulent flow. The higher order velocity structure functions of order m were measured and modeled using the sweeping decorrelation hypothesis. In order to reduce the influence of Taylor's frozen hypothesis on the assessment of the sweeping decorrelation hypothesis, two dimensionless quantities, developed by Praskovsky et al. (1993), were used. Based on these dimensionless quantities, the sweeping decorrelation hypothesis predictions agreed well with the higher order structure function measurements. Assumptions inherent in the sweeping decorrelation hypothesis were also considered. It was found that strong interaction existed between the energy containing scales and the inertial subrange scales, indicating that the sweeping action alone does not fully describe the higher order structure function. Also, local temperature-velocity interactions were measured and found to be significant thus weakening the validity of the sweeping decorrelation hypothesis. However, these two interaction mechanisms appeared to be opposite in sign and counteracted each other.

1. Introduction

The statistical structure of the inertial subrange is commonly derived from dimensional arguments proposed by Kolmogorov (1941) (referred to in this study as K41). In K41, the velocity spectrum is taken to be a function of only the mean rate of energy transfer per unit mass (assumed to be identical to the mean turbulent kinetic energy (TKE) dissipation rate per unit mass $\langle\varepsilon\rangle$), and the wavenumber ($K$). These dimensional arguments result in the well known $-5/3$ power law

$$E(K) = C_1\langle\varepsilon\rangle^{2/3} K^{-5/3}, \tag{1}$$

where C_1 is the Kolmogorov constant.

In order to test whether these dimensional arguments also hold for higher order velocity spectra in the atmosphere, Dutton and Deaven (1972) considered the spectra of algebraic powers of

SSDI 0169-5983(95)00011-9

velocity fluctuations defined by

$$\langle (u_i^m - \langle u_i^m \rangle)^2 \rangle = \int_{K_1}^{K_2} E_i^{(m)}(K)\, \mathrm{d}K, \tag{2}$$

where $E^{(m)}(K)$ is the power spectrum of order (m), $\langle\ \rangle$ is the averaging operator, and u_i are the velocity fluctuations about the time averaged velocity components U_i. Here, subscript $i = 1, 2$, and 3 represent the longitudinal, lateral, and vertical directions, respectively, and $\langle u_i \rangle = 0$. Dutton and Deaven argued that if (1) holds, then the same dimensional analysis should be applicable to $E^{(m)}(K)$ within the inertial subrange. This dimensional analysis results in

$$E_i^{(m)}(K) = C_m \langle \varepsilon \rangle^{2m/3} K^{-(2m+3)/3}, \tag{3}$$

where C_m are constants to be determined (C_1 is the Kolmogorov constant). Hence, $E^{(1)} \sim K^{-5/3}$, $E^{(2)} \sim K^{-7/3}$, etc.

To investigate the validity of (3), Dutton and Deaven measured higher-order spectra (up to $m = 4$) for all velocity components at four different elevations above the land surface. The measurements were carried out in the atmospheric surface layer (ASL), the atmospheric boundary layer (ABL), and for clear air turbulence (CAT) conditions. They found that the higher-order ($m > 1$) velocity spectra depart significantly from predictions by (3) and appeared to follow the $-5/3$ power law in the inertial subrange for all m. Dutton and Deaven interpreted these results as evidence that an inertial subrange, in the atmosphere, is not only defined by $\langle \varepsilon \rangle$ and K. Motivated by the results of Dutton and Deaven, Van Atta and Wyngaard (1975) investigated the higher-order velocity spectra of ABL measurements over the ocean. They showed that, for a Gaussian velocity distribution, the higher order velocity spectra follow

$$E_{u_i}^{(m)}(K) = m^2 (1 \times 3 \times 5 \times .. \times 2m - 1) \langle u_i^2 \rangle^{m-1} E_{u_i}^{(1)}(K). \tag{4}$$

Notice that the above equation is different from (3) since it involves $\langle u_i^2 \rangle$ in the inertial subrange (and not simply $\langle \varepsilon \rangle$ and K). Notice that for $m = 1$, (4) is consistent with K41. Measurements of higher order velocity spectra in the ABL over the ocean seem to confirm (4) despite some observed departure from Gaussian velocity distributions (see Van Atta and Wyngaard, 1975).

A related problem was studied by Tennekes (1975) who investigated the relationship between the Eulerian and Lagrangian velocity spectra for isotropic zero-mean turbulent flow. Tennekes (1975) assumed that small eddies (i.e. eddies much smaller than the energy-containing eddies) are transported past a Eulerian observer without any dynamical distortion (here after referred to as sweeping). As suggested by Tennekes, these arguments are analogous to Taylor's (1938) frozen turbulence hypothesis. Unlike Taylor's hypothesis, the transport of the small scales is not related to the mean flow but to the energy content of the larger eddies. That the small eddies are not distorted by the energy containing eddies can be attributed to the absence of any statistical interaction between the two scales of motion. The absence of such an interaction is central to the concept of inertial energy-cascade. Tennekes found that if this "sweeping" action occurs, then the large scale eddies must be directly contributing to the kinetic energy per unit mass of the smaller scales within the Eulerian inertial subrange (i.e. the small scales are in motion because of the kinetic energy of the larger scales). Therefore, the kinetic energy per unit mass of the larger scales ($\langle u_i^2 \rangle$) should be considered in the dimensional analysis of the inertial subrange in the Eulerian framework. Based

on this argument, the Eulerian frequency spectra for u_i^2 may be described as

$$E_{u_i}^{(2)}(f) = \alpha_i \langle \varepsilon \rangle^{2/3} \langle u_i^2 \rangle^{1/3} f^{-5/3}, \tag{5}$$

where f is the frequency, and α_i are unknown constants to be determined. The fact that $\langle u_i^2 \rangle$ influences the dynamics of the inertial subrange has important implications to turbulence models. This is due, in part, to the fact that current approaches to modeling velocity and scalar statistics in the inertial-subrange assume complete independence between the energy-containing eddy motion and the inertial subrange. Tennekes (1975) supported his arguments regarding the importance of sweeping by comparing the differences between the Eulerian and Lagrangian correlation time scales from low Reynolds number isotropic grid generated turbulence measurements reported by Comte-Bellot and Corrsin (1971), and Shlien and Corrsin (1974). Tennekes's arguments are also in agreement with the data reported by Van Atta and Wyngaard (1975).

Interest in the Tennekes (1975) hypothesis (hereafter referred to as the sweeping decorrelation hypothesis (SDH)) was renewed by the theoretical study of Yakhot et al. (1989). Based on renormalization group theory (RNG) analysis (see e.g. McComb, 1991), Yakhot et al. (1989) found that $E^{(2)} \sim K^{-7/3}$, which can also be obtained from straightforward extension of the original Kolmogorov scaling arguments as was earlier done by Dutton and Deaven (1972). That is, RNG analysis seems to support the arguments leading to (3). The $-5/3$ power-law generally observed in the higher order velocity spectra may be due to the use of Taylor's hypothesis (see Yakhot et al., 1989; Praskovsky et al., 1993). Based on the RNG analysis, Yakhot et al. concluded that sweeping, in the sense of Tennekes (1975), is not important for the Eulerian inertial subrange.

The same topic was considered in great depth by Praskovsky et al. (1993). Based on high Reynolds number wind tunnel shear and mixing layer velocity measurements, they concluded that the scaling arguments in (4) or (5) appear to match the measurements. However, important assumptions leading to the SDH were violated. Namely, Praskovsky et al. (1993) measured strong interaction between the energy-containing scales and the inertial subrange scales. The presence of this interaction has important consequences for both large-Eddy simulations (LES) and energy cascade models. For example, current LES neglect this interaction at the outset. Furthermore, this interaction has important consequences on energy cascade models, intermittency corrections to Kolmogorov's theory (see e.g. Kuznetsov et al. 1992), and local isotropy assumptions. This interaction also implies that the SDH cannot be exact since this interaction implies that the small scales are distorted by the larger scales. Table 1 summarizes results from several numerical experiments related to the applicability (and adequacy) of the sweeping decorrelation hypothesis. Many more theoretical investigations based on order of magnitude analysis or numerical simulations of the Navier–Stokes equations (NS) have been reported in the literature but will not be reviewed here.

It is these issues and the important experimental findings of Praskovsky et al. (1993) that motivated the present investigation of the higher-order spectra and the random sweeping decorrelation hypothesis in the unstable ASL. In this study, 56 Hz triaxial sonic anemometer velocity measurements were carried out at 2–3 m above a uniform dry lakebed that extends some 14 km in the North–South direction and 4 km in the East–West direction for a wide range of atmospheric stability conditions. In the ASL, the temperature disturbances are typically large even when the net sensible heat flux is small. These large temperature fluctuations can potentially induce significant deviations from the SDH predictions since the eddies that are transported past a Eulerian observer

Table 1
Summary of some sweeping decorrelation hypothesis (SDH) investigations

Authors	Analysis	Key conclusion
Yakhot et al. (1989)	Renormalized group theory (RNG)	Sweeping is not important for the Eulerian higher order velocity power spectrum.
Nelkin and Tabor (1990)	Order of magnitude analysis of NS	SDH is: (a) invalid if TKE spectrum scales as static Pressure spectrum (see Monin and Yaglom, 1975 pp. 407), and (b) valid if TKE spectrum scales as $K^{-5/3}$
Chen and Kraichnan (1989)	Numerical simulations	RNG analysis is ill-suited for analyzing the importance of sweeping.
Sanada and Shanmugasundaram (1992)	Numerical simulations of NS	The sweeping time (characterizing the small scale convection by the large energy containing scale) is more important than the local inertial eddy-turnover time in determining the form of the TKE spectrum in isotropic turbulence.
McComb et al. (1989)	Numerical simulations of NS	The inertial eddy-turnover time is dominant in high Reynolds number decaying turbulence.

The analysis performed to assess the validity of SDH and resulting key conclusions are also listed. NS stands for Navier Stokes equations.

are not only distorted by large-scale/inertial subrange interaction (as confirmed by Praskovsky et al., 1993) but also by the local velocity/thermal interaction.

The specific objectives of this study are : (i) to assess the adequacy of the SDH in ASL flows using the structure function approach, and (ii) to examine the assumptions intrinsic to the SDH using the methods developed by Praskovsky et al. (1993) with emphasis on large-scale/small-scale interactions with possible thermal distortions over a wide range of atmospheric stability conditions. First, we briefly review the SDH using the structure function approach.

2. Higher order spectra and structure functions

The higher order structure function $D^{(m)}(r)$ as defined by Dutton and Deaven is given by

$$D^{(m)}(r) = \langle [u_i^m(x_1 + r) - u_i^m(x_1)]^2 \rangle, \tag{6}$$

where x_1 is the coordinate direction along the mean horizontal wind speed, and r is the separation distance along x_1 between two points in the inertial subrange. Replacing the velocity difference $\Delta u_i = u_i(x_1 + r) - u_i(x_1)$ in $D^{(m)}(r)$ and expanding, we obtain

$$\begin{aligned} D^{(m)}(r) &= \langle [(u_i + \Delta u_i)^m - u_i^m]^2 \rangle \\ &= m^2 \langle u_i^{2m-2} \Delta u_i^2 \rangle + m^2(m-1) \langle u_i^{2m-3} \Delta u_i^3 \rangle \\ &\quad + m^2(m-1)\tfrac{1}{12}(7m-11) \langle u_i^{2m-4} \Delta u_i^4 \rangle + \dots . \end{aligned} \tag{7}$$

To avoid confusion, we note the difference between the higher order structure function in (6) and (7) and the traditional nth order structure function defined by $D^{(n)}(r) = \langle \Delta u_i^n \rangle$.

Praskovsky et al. (1993), demonstrated that (7) reduces to

$$D^{(m)}(r) = m^2 \langle [u_i^{2m-2} \rangle \langle [u_i(x_1 + r) - u_i(x_1)]^2 \rangle, \tag{8}$$

if the following assumptions are invoked:

(i) K41 and all assumptions associated with K41 (e.g. local isotropy, high Reynolds numbers) are valid so that the traditional structure function scales as

$$\langle \Delta u^m \rangle = C_m (\langle \varepsilon \rangle r)^{m/3}. \tag{9}$$

(ii) The SDH is valid. This hypothesis is necessary to simplify terms involving $\langle u_i^k \Delta u_i^l \rangle$ in (7). In general, these terms can be expanded as

$$\langle u_i^k \Delta u_i^l \rangle = \langle u_i^k \rangle \langle \Delta u_i^l \rangle + \rho_{k,l} \sigma_{u^k} \sigma_{\Delta u^l}, \tag{10}$$

for any arbitrary powers k and l, with the correlation coefficient $\rho_{k,l}$ defined by

$$\rho_{k,l} = \frac{\langle (u_i^k - \langle u_i^k \rangle)(\Delta u_i^l - \langle \Delta u_i^l \rangle) \rangle}{\sigma_{u^k} \sigma_{\Delta u^l}} \tag{11}$$

and σ_x is the root-mean square value of any variable x defined by

$$\sigma_x = [\langle (x - \langle x \rangle)^2 \rangle]^{1/2}. \tag{12}$$

The "sweeping" event is based on the assumption that large scale and inertial subrange scales are statistically independent (i.e. no dynamical distortion of inertial subrange scales as they sweep past a Eulerian observer). Praskovsky et al. (1993) showed that this assumption leads to $\rho_{k,l} = 0$ if the following arguments are invoked: (i) Δu_i is a characteristic velocity for the inertial subrange eddy motion. (ii) u_i is a characteristic velocity for the large scale eddy motion.

Hence, with $\rho_{k,l} = 0$, quantities involving $\langle u_i^k \Delta u_i^l \rangle$ simplify to $\langle u_i^k \rangle \langle \Delta u_i^l \rangle$. Upon Fourier transforming (8), one obtains the higher order velocity spectra $E^{(m)}(K)$

$$E_i^{(m)}(K) = m^2 \langle u_i^{(2m-2)} \rangle E^{(1)}(K). \tag{13}$$

Based on K41, the inertial subrange energy spectrum is given by $E^{(1)}(K) = C_1 \langle \varepsilon \rangle^{2/3} K^{-5/3}$ so that (13) reduces to

$$E_i^{(m)}(K) = C_1 m^2 \langle u_i^{(2m-2)} \rangle \langle \varepsilon \rangle^{2/3} (K)^{-5/3}, \tag{14}$$

which shows that the higher order velocity spectra within the inertial subrange are influenced by the large scale energy (e.g. $\langle u_i^{2m-2} \rangle$), and the power-law behavior (i.e. $-5/3$) is independent of the order (m) in agreement with Van Atta and Wyngaard (1975).

3. Experimental setup

An experiment was carried out on June 22–29, 1993 over a dry lakebed (Owens lake) in Owens Valley, California. The lakebed is contained within a large basin bounded by the Sierra Nevada range and the White and Inyo Mountains. The experimental site is located on the northeast portion of the lakebed (elevation = 1100 m). The site's surface is a smooth heaved sandy soil extending uniformly in excess of 10 kilometers in all directions. The three velocity components and temperature (T) were measured using a triaxial ultrasonic anemometer (Gill Instruments, Model 1012R2). Sonic anemometers measure the three velocity components by sensing the effect of wind on the transit times of sound pulses traveling in opposite directions across a known instrument path distance d_{sl}(= 0.149 m in this study). The sonic anemometer is suited for this experiment since

it is relatively free of calibration nonlinearities, atmospheric contamination problems and calibration drifts, and time lag responses. As shown by Wyngaard (1981), the main disadvantage of sonic anemometers is the wavenumber distortion due to averaging along the finite sonic path. This distortion is restricted to wavenumbers in excess of $2\pi/d_{sl}(=42.2\ \mathrm{m}^{-1})$. The sampling frequency (f_s) and the sampling period (T_p) were 56 Hz and 15 minutes, respectively, resulting in 50400 measurements per velocity component. Taylor's (1938) hypothesis was used to convert the time domain to space or wavenumber domain. We focus here on two runs that represent near-neutral and unstable atmospheric conditions. These two runs were selected because the (i) velocity time series can be decomposed without ambiguity into a mean and a fluctuating part, (ii) turbulent intensity was relatively small when compared to other runs, (iii) resolved inertial subrange by the sonic anemometer extends over two decades of scales, and (iv) integral time scales were very small (3%) when compared to the sampling period. These criteria were necessary to (i) eliminate any ambiguity regarding steadiness in the mean meteorological conditions and the contribution of turbulence to the time series, (ii) ensure the validity of Taylor's hypothesis, at least for inertial subrange scales, (iii) ensure the availability of a significant number of sample points for power-law determination within the inertial subrange, and (iv) ensure the convergence of time averaging to ensemble averaging. Figs. 1a and 1b display the time series ($N = 50400$ points) of the longitudinal velocity and temperature for these two runs. Notice in Fig. 1a that peak to mean velocity ratios of up to 2.0 were measured. It is evident from Fig. 1b that the temperature fluctuations for Run 1 (unstable conditions) were much larger in magnitude than for Run 2 (near-neutral) and exhibit a ramp-like pattern consistent with many shear-flow experiments.

The measured turbulence conditions for these runs are displayed in Table 2. In Table 2, the integral length scale (L_u), the Taylor microscale (λ), and the Kolmogorov dissipation scale (η) were estimated from

$$L_u = \frac{\langle U_1\rangle}{\langle u_1^2\rangle}\int_0^{\infty}\langle u_1(t+\tau)u_1(t)\rangle\,\mathrm{d}\tau, \qquad \lambda = \frac{\sigma_{u_1}\langle U_1\rangle}{\langle[\partial u_1/\partial t]^2\rangle^{1/2}}, \qquad \eta = \left[\frac{\nu^3}{\langle\varepsilon\rangle}\right]^{1/4}, \tag{15}$$

where ν is the air kinematic viscosity. For determining L_u, the integration in (15) was carried out up to the first zero crossing as discussed in Sirivat and Warhaft (1983). The determination of the time derivative in λ was carried out after a cubic spline interpolation scheme was applied to the velocity time series. It should be noted that the validity of Taylor's hypothesis, the local isotropy assumption, and the insufficient sampling resolution may strongly influence the accuracy of λ. However, this is not very crucial since λ is only reported here to provide an estimate of the Taylor microscale Reynolds number (Re_λ) for comparisons with other studies. This information is not needed for evaluating the SDH as long as Re_λ is sufficiently large.

To further compare our results with other studies, the dissipation rate was estimated from the local isotropy relation

$$\langle\varepsilon\rangle = 15\nu\langle[\partial u_1/\partial x_1]^2\rangle. \tag{16}$$

The space derivative can be computed from the time derivative using Taylor's hypothesis. Due to the volume averaging of the sonic anemometer, the $\langle\varepsilon\rangle$ estimated from the mean square velocity gradient might be smaller than the true value. Hence, we also estimated the dissipation rate using (1) with $C_1 = 0.55$ (see e.g. Kaimal and Finnigan, 1994, and Wyngaard and Pao, 1972) to assess the

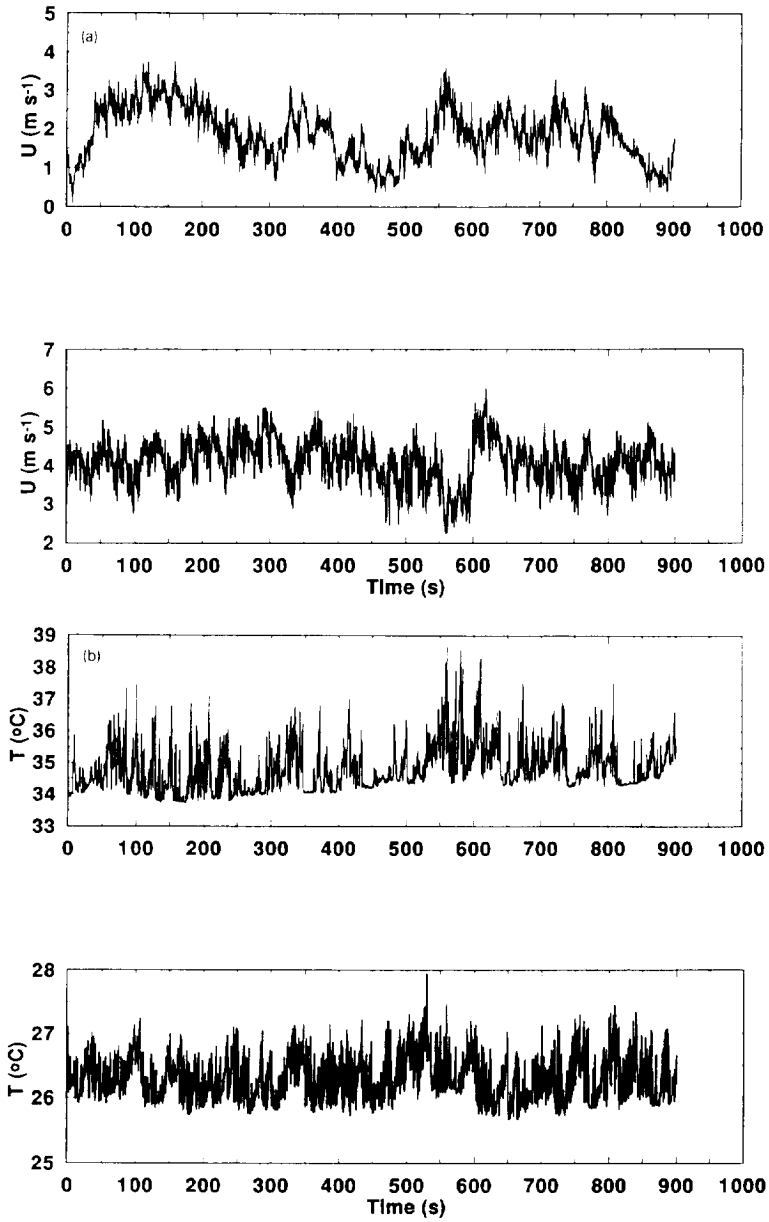

Fig. 1. (a) Longitudinal velocity time series measurements for Runs 1 (upper), and 2 (lower). (b) Air temperature time series measurements for Runs 1 (upper) and 2 (lower).

adequacy of (16). The agreement between the two dissipation rate estimates was good considering that the sonic path length ($d_{sl} = 0.149$ m) is comparable to λ (see Table 2). Fig. 2a shows the measured power spectra for Runs 1 and 2 as well as the Kolmogorov spectrum. The dissipation rate in Fig. 2a was determined from (16). Fig. 2a suggests that the $-5/3$ power law covers at least

Table 2
Summary of measured mean meteorological and turbulence conditions

Run description		
Run #	1	2
Day of year (1993)	178	180
Starting time (PDST)	08:53	07:42
Mean meteorological conditions		
Net radiation (R_n), W m^{-2}	227	94
Sensible heat flux (H), W m^{-2}	105	38
Long. velocity (U_1), m s^{-1}	1.86	4.09
Mean air temperature (T_a), C	34.8	26.3
Turbulence statistics		
Root-mean square velocity (σ_{u1}), m s^{-1}	0.665	0.533
Root-mean square velocity (σ_{u2}), m s^{-1}	0.589	0.530
Root-mean square velocity (σ_{u3}), m s^{-1}	0.270	0.211
Root-mean temperature (σ_T), C	0.51	0.18
Mean Dissipation Rate ($\langle\varepsilon\rangle \times 10^3$) m^2 s^{-3}		
(i) Using local isotropy relation	2.5	3.3
(ii) Using power spectrum (E_{u1})	3.1	4.1
Turbulent intensity (I_{u1})	0.36	0.13
Length scales		
Measurement height (z), m	3.0	2.25
Obukhov length (L_{MO}), m	− 2.5	− 13.2
Integral length scale (L_u), m	61	43
Taylor microscale (λ), m	0.257	0.139
Kolmogorov dissipation scale (η), mm	1.22	1.01
Flow properties		
Reynolds number (Re_λ)	11,398	4,953
Scale separation (L_u/η) × 10^5	0.50	0.43
Atmospheric stability parameter (z/L_{MO})	− 1.2	− 0.17
Inertial subrange (m)	0.15 25	0.15 − 10

The experiment starting time is in Pacific daylight saving (PDST).

two decades of wavenumbers. Also, it does suggest that the estimate $\langle\varepsilon\rangle$ is sufficiently accurate for the purpose of this study. In Fig. 2b the measured power spectra for the temperature time series are also presented. It should be noted that departures from K41 scaling (i.e. − 5/3 power law) is noted in Fig. 2b for the temperature time series. A summary of these estimates is presented in Table 2.

Finally, from Table 2, we note that the atmospheric stability parameter (z/L_{MO}) varied by about an order of magnitude. Here, L_{MO} is the Obukhov length given by

$$L_{MO} = \frac{-\rho u_*^3}{kg[H/c_P T_a]}. \tag{17}$$

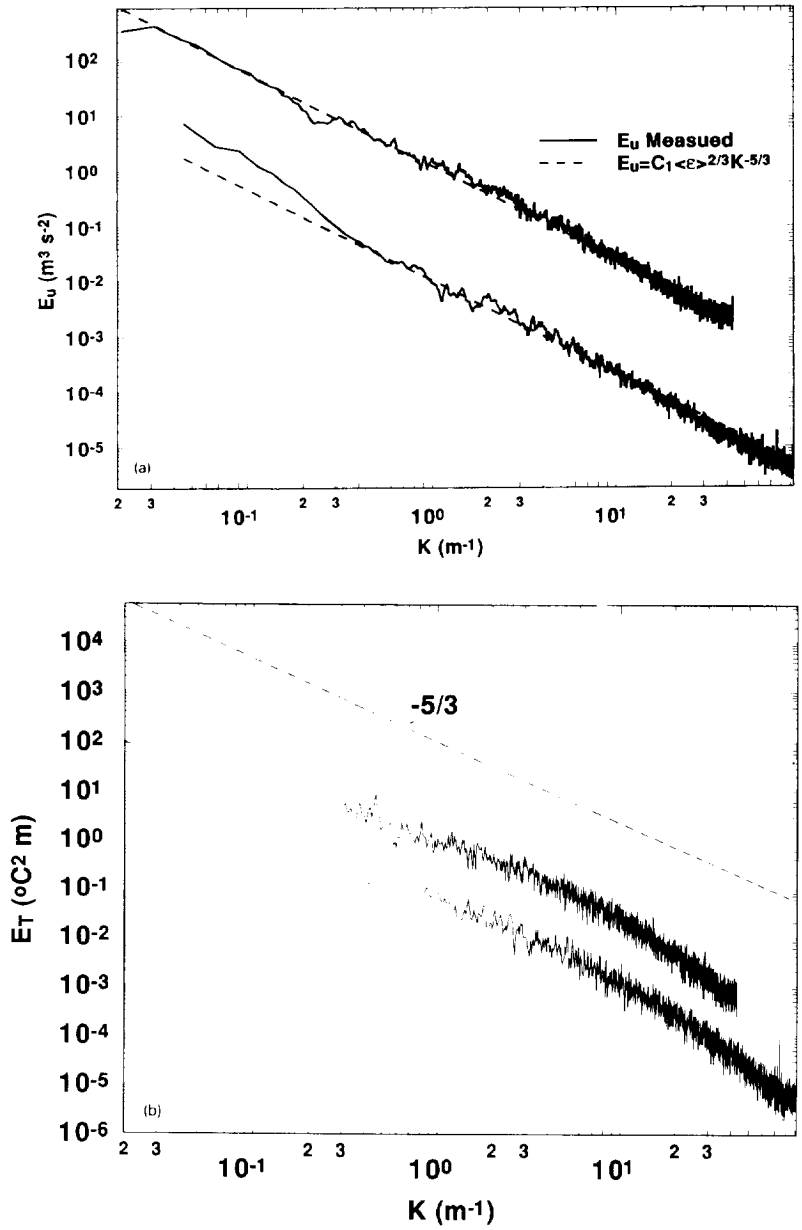

Fig. 2. (a) Longitudinal velocity power spectra $E_u(K)$ from Runs 1 and 2. To permit comparison, Run 2 was shifted by two decades along the ordinate axis. The dissipation rate in $E_u(K) = C_1\langle\varepsilon\rangle^{2/3}K^{-5/3}$ (dotted line) was estimated from the local isotropy relation. (b) Same as (a) but for the temperature time series.

where u_* is the friction velocity, H is the sensible heat flux, T_a is the mean air temperature, g is the gravitational acceleration, $k(=0.4)$ is Von Karman's constant, ρ is the air density, and c_p is the specific heat capacity of dry air under constant pressure. Other supporting measurements such as net radiation (R_n), H, and T_a are also presented in Table 2. Further details regarding the

experimental setup and the use of the sonic anemometer to measure the temperature fluctuations can be found in Katul et al. (1994 a, b).

4. Results and discussion

The results and discussion section is divided into three parts. The first part identifies the inertial subrange that is used to investigate the SDH for Runs 1 and 2; the second part presents an assessment of the SDH for a wide range of atmospheric stability conditions; and the third part examines possible statistical interaction between large and inertial scales. Recall that the SDH neglects this interaction, and hence, this analysis investigates an important assumption.

4.1. Identification of the inertial subrange

The inertial subrange was identified from the dependence of the traditional third order structure function on r using

$$\langle \Delta u_1)^3 \rangle = -\tfrac{4}{5}\langle \varepsilon \rangle r \tag{18}$$

(see Landau and Lifshitz, 1987; Monin and Yaglom, 1975 Ch. 8). The identification of the inertial subrange using the traditional third order structure function is more accurate than the $-5/3$ power spectrum approach since:

(i) Internal intermittency does not affect the scaling.

(ii) The third order structure function is a higher moment than the power spectrum (second moment) and is therefore more sensitive to small deviations from inertial subrange behavior (see e.g. Anselmet et al., 1984).

(iii) The convergence of the measured third order structure function to (18) requires a much larger sample size than the convergence of the power spectrum to (1). Hence, the convergence of the measured $\langle \Delta u_1{}^3 \rangle$ to the result in (18) serves as an indirect check on the adequacy of the sample size.

(iv) The log-intercept in (18) can also serve as an independent check on the estimated dissipation rate from (16).

Figs. 3a and 3b display the measured $\langle \Delta u_1^3 \rangle$ and the inertial subrange as identified by (18) for Runs 1 and 2, respectively. Eq. (18) with $\langle \varepsilon \rangle$ determined from the local isotropy relation is also shown (dotted line). Good agreement between (18) and the measured $\langle \Delta u_1^3 \rangle$ is noted. The measured $\langle \Delta u_1^3 \rangle$ at small r (< 0.15 m) is not reliable due to possible sonic anemometer distortions. Hence, we restrict the statistical analysis to r larger than d_{st}($= 0.149$ m). The inertial subrange limits (dotted vertical lines) as well as L_u are also displayed in Figs. 3a and 3b.

4.2. Evaluation of the sweeping-decorrelation hypothesis and higher-order spectra

The higher order spectra for Runs 1 and 2 are displayed in Figs. 4a and 4b for $m = 2$–4, respectively. These higher order spectra are formally defined by

$$E_{u_1}^{(m)}(f) = \int_{-\infty}^{+\infty} \langle u_1^m(t)\, u_1^m(t+\tau) \rangle \mathrm{e}^{-\mathrm{i}2\pi f\tau}\, \mathrm{d}\tau, \tag{19}$$

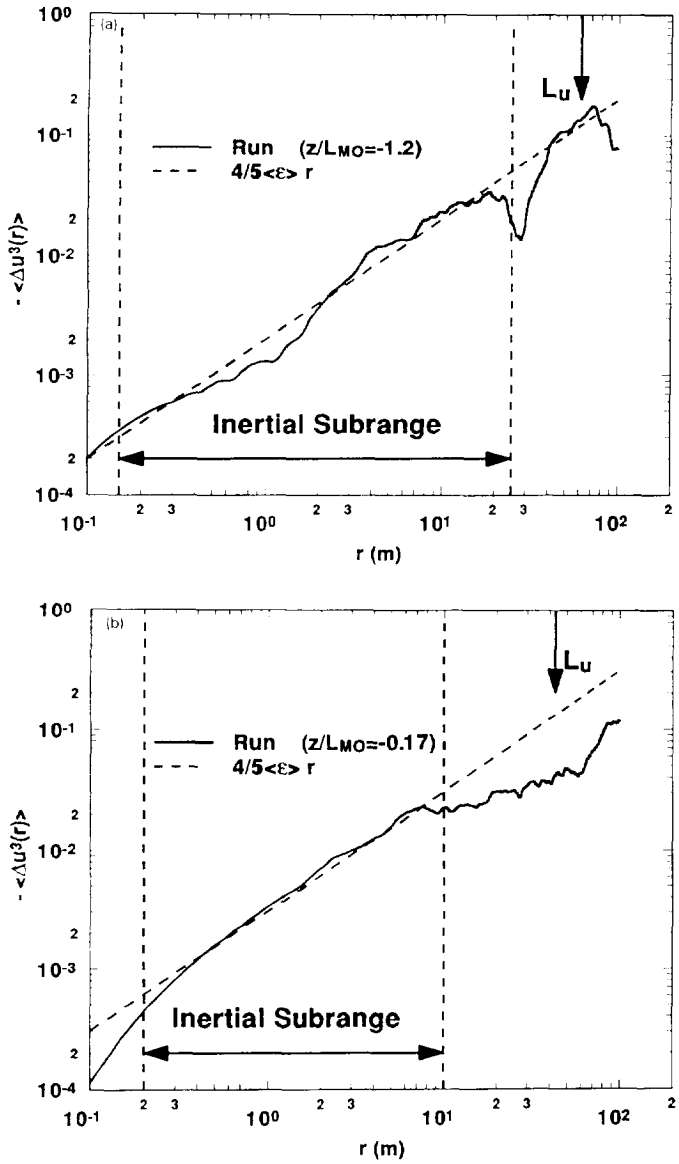

Fig. 3. (a) Identification of the inertial subrange for Run 1 using the dependence of the third order structure function ($\langle \Delta u_1^3 \rangle$) on r. The dotted line is the $\langle \Delta u_1^3 \rangle = -4/5 \langle \varepsilon \rangle r$. The dissipation rate is from the local isotropy relation. The inertial subrange scales are between the two vertical lines. For $r < 15$ cm, the sonic anemometer distortion due to finite path length becomes critical. (b) Same as (a) but for Run 2.

where f is the frequency, and τ is the time lag. However, the calculations of the higher order spectra were carried out as follows. (i) Construct the u_1^m time series from u_1 time series measurements. (ii) Subtract the mean $\langle u_1^m \rangle$ to generate a zero-mean u_1^m time series. (iii) Determine the power spectrum for the series in step 2. (iv) Band average the results of step (3) for smoothing the spectra to better reveal power-laws.

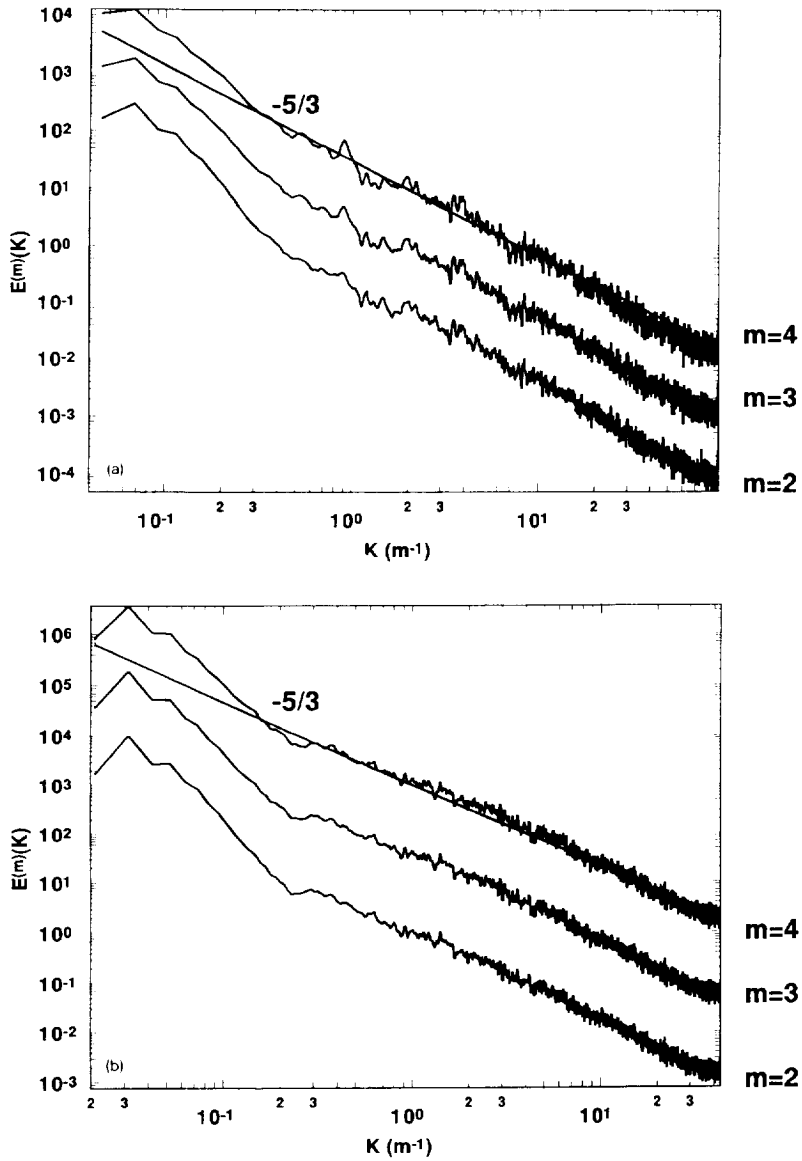

Fig. 4. (a) The evolution of the higher order spectra $E^{(m)}$ as a function of wavenumber K for $m = 2$ to 4 for Run 1. For comparison with RNG power-law predictions, the $-5/3$ power law is also shown (dotted line). (b) Same as (a) but for Run 2.

In our study, the power spectrum was calculated by dividing the 50400 u_1^m points into 6 windows, each of length 8192 points, cosine tapering 5% on each window side, fast fourier transforming the time series measurements within each window using FFT, computing the amplitudes of the Fourier coefficients per unit wavenumber for all wavenumbers in each window, and then averaging the spectra of all six windows. The frequency was converted to wavenumber (K) using Taylor's

hypothesis ($K = 2\pi f/U_1$). The higher order spectra of Figs. 4a and 4b clearly do not support the scaling arguments $E^{(2)} \sim K^{-7/3}$, $E^{(3)} \sim K^{-3}$, $E^{(4)} \sim K^{-11/3}$ and appear to exhibit a near $-5/3$ power law for inertial subrange wavenumbers in agreement with other higher order spectra reported by Dutton and Deaven (1972) and Van Atta and Wyngaard (1975). Although these spectra do not follow $E^{(2)} \sim K^{-7/3}$, $E^{(3)} \sim K^{-3}$, $E^{(4)} \sim K^{-11/3}$, they do not prove the validity of the SDH.

As discussed in Praskovsky et al. (1993), a better quantity for assessing the validity of the SDH is

$$d^m(r) = \frac{D^{(m)}(r)}{m^2\langle u_1^{2m-2}\rangle\langle (u_1(x+r) - u_1(x))^2\rangle} = 1. \tag{20}$$

The above equation is derived from the ratio of (6) to (8). Notice that (20) is not as sensitive to Taylor's frozen hypothesis as the higher-order spectra defined by (19). This insensitivity can be attributed to the differencing operation in the numerator and denominator. Any distortion caused by Taylor's hypothesis affects both numerator and denominator, and hence, must have less influence on their ratio. If the SDH is valid, then $d^{(m)}(r) = 1$ for all r within the inertial subrange. Figs. 5a, 5b, and 5c show the variation of $d^{(m)}$ with r for Runs 1 and 2 within the inertial subrange for $m = 2, 3,$ and 4, respectively. We should note that (20) involves two separate averaging operations, one in the numerator and the other in the denominator, and therefore might still be partially sensitive to Taylor's hypothesis. What is important to note in Figs. 5a to 5c is that $d^{(m)}(r)$ is systematically less than unity. Based on the structure function approach utilized in section 2, $d^{(m)}(r)$ should be greater than unity within the inertial subrange since the SDH neglects all but the first term in (7). If these terms are significant, then (6) must be larger than (8) for all r within the inertial subrange and $d^{(m)}(r)$ must be larger than unity. The data presented in Praskovsky et al. (1993)

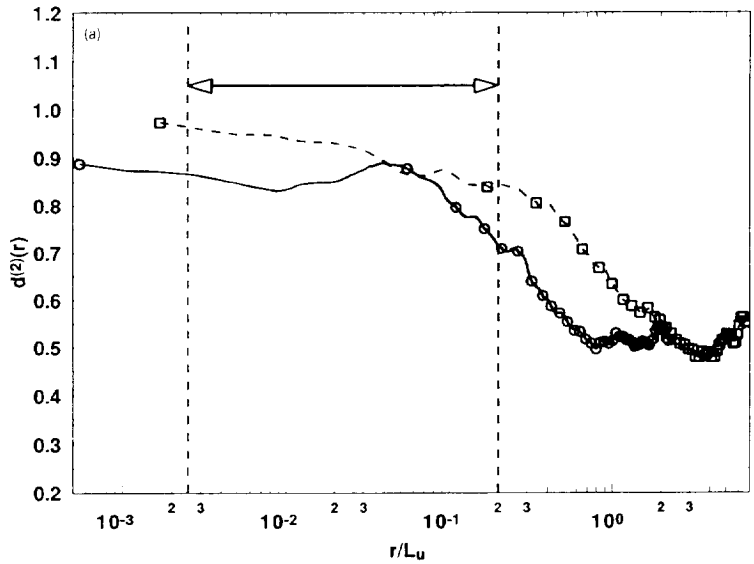

Fig. 5. (a) The variation of $d^{(m)}(r)$ as a function of r for $m = 2$ and Runs 1 (empty circle) and 2 (empty square). The vertical dotted lines denote the inertial subrange. The sweeping decorrelation is valid if $d^{(m)}(r) = 1$. The labeling is performed once for every 100 sequential measurements. (b) Same as (a) but for $m = 3$. (c) Same as (a) but for $m = 4$.

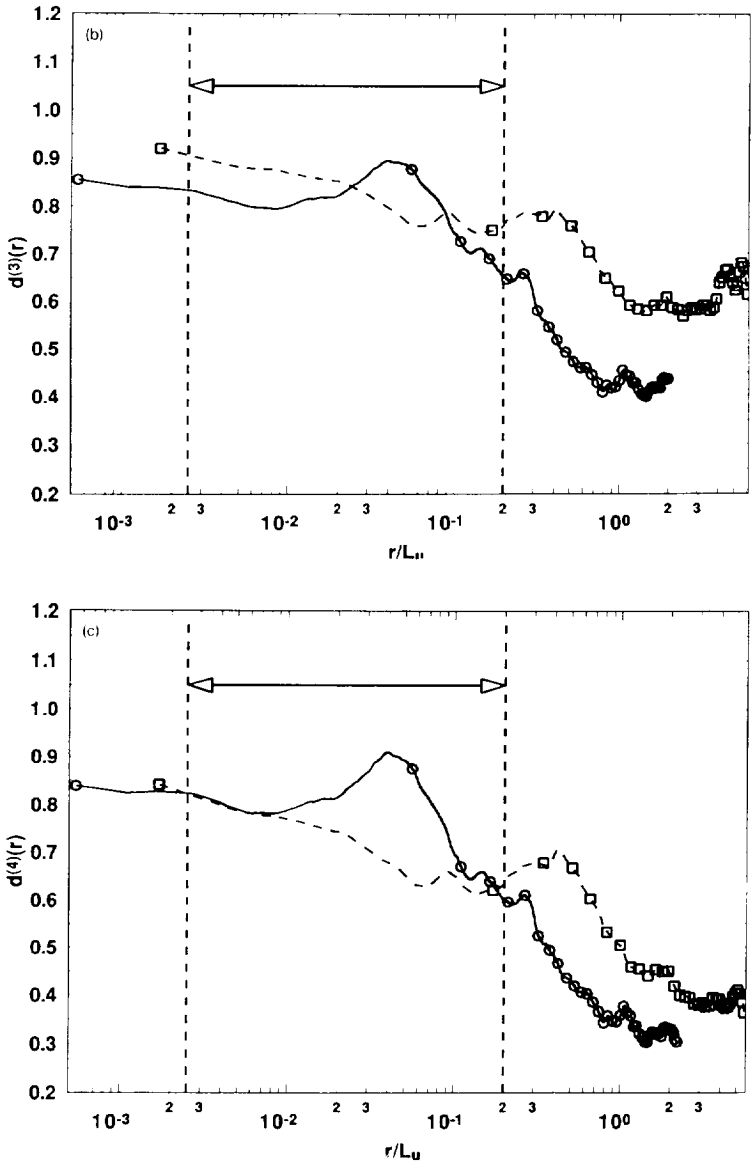

Fig. 5. (continued)

(specifically Fig. 2 in their study) confirms $d^{(m)}(r)$ is always greater than unity, which is not in agreement with Figs. 5a–5c. Possible local velocity–temperature interactions may be responsible for the reduction in $d^{(m)}$ and will be discussed in the following section.

In order to compare our results with the laboratory data of Praskovsky et al. (1993), another dimensionless measure for assessing the adequacy of the SDH is computed

$$g^m(r) = \left\langle \frac{[u_1^m(x+r) - u_1^m(x)]^2}{[u_1(x+r) - u_1(x)]^2} \right\rangle \left[\frac{1}{m^2 \langle u_1^{2m-2} \rangle} \right] = 1 \tag{21}$$

and invokes assumptions identical to (20). However, a key advantage to (21) is attributed to the one averaging operator that also involves differencing in the numerator and denominator, respectively, at the same location x (or time t). Thus the influence of Taylor's hypothesis on $g^{(m)}(r)$ must be even smaller than its effect on $d^{(m)}$ (or negligible). Also, since $g^{(m)}$ involves one averaging operator, it is more sensitive to atmospheric stability effects than $d^{(m)}(r)$. Figs. 6a–6c show the variation of $g^{(m)}$ with r in the inertial subrange for $m = 2$, 3, and 4, respectively. For small m, $g^{(m)}$ is nearly

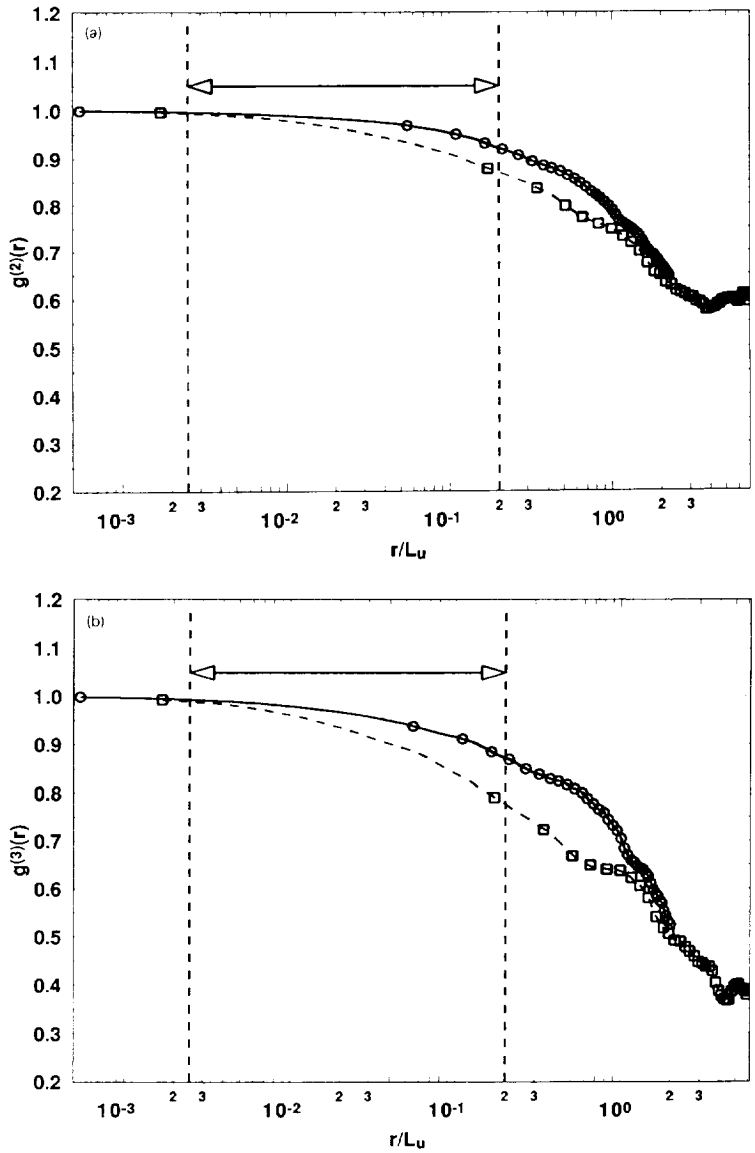

Fig. 6. (a) Same as Fig. 5a but for $g^{(m)}(r)$. (b) Same as Fig. 5a but for $m = 3$ and $g^{(m)}(r)$. (c) Same as Fig. 5a but for $m = 4$ and $g^{(m)}(r)$.

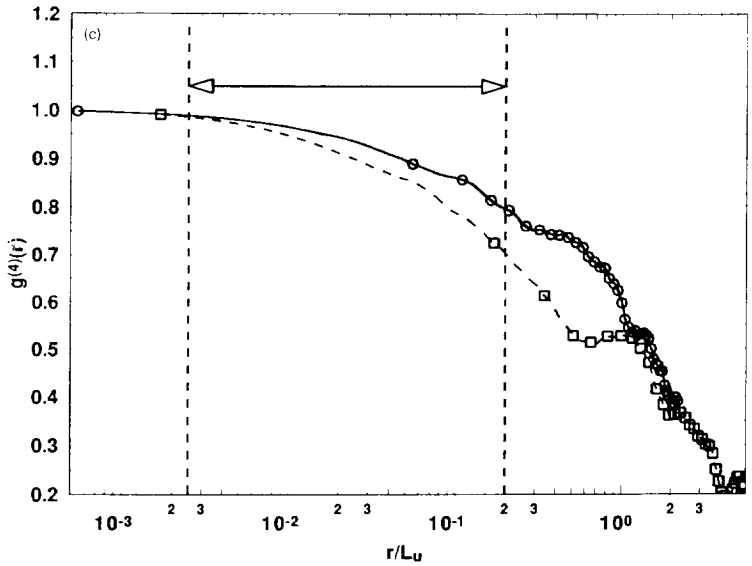

Fig. 6. (continued)

unity for all values of r in the inertial subrange and agrees with the $g^{(m)}$ data in Praskovsky et al. (1993). It is interesting to note that the $g^{(m)}$ deviations from unity are systematically higher for near-neutral conditions (Run 2) when compared to the unstable conditions (Run 1). This point deserves further analysis and is discussed in the following section.

We note that the variation of $d^{(m)}$ and $g^{(m)}$ within the inertial subrange are of the same magnitude. Hence, errors due to Taylor's hypothesis are small since Taylor's hypothesis cannot influence both quantities in the same fashion. Figs. 6a and 6b also indicate that as m increases, some deviations from unity are noted for the larger inertial subrange scales. We investigate next whether these deviations from unity are due to large-scale/inertial-scale interaction and/or local thermal/velocity interactions.

4.3. Large-scale inertial-scale interaction

The interaction between the large scale excitation and the inertial scale excitation within inertial subrange r can be evaluated from the correlation coefficient

$$\rho_{k,l} = \frac{\langle (u_i^k - \langle u_i^k \rangle)(\Delta u_i^l - \langle \Delta u_i^l \rangle) \rangle}{\sigma_{u^k} \sigma_{\Delta u^l}}. \tag{22}$$

If this correlation is significant, then quantities involving $\langle u_i^k \Delta u_i^l \rangle$ do not simplify to $\langle u_i^k \rangle \langle \Delta u_i^l \rangle$ and the sweeping decorrelation hypothesis of (8) is no longer valid. For that purpose, we computed $\rho_{2,2}$ and $\rho_{4,4}$ as a function of r for both runs. The evolution of these correlations with r for both runs are shown in Figs. 7a and 7b for $m = 2$ and 4, respectively. It is evident from these figures that the correlations are not small and are in fact very comparable to the dimensionless correlations reported in Praskovsky et al. (1993).

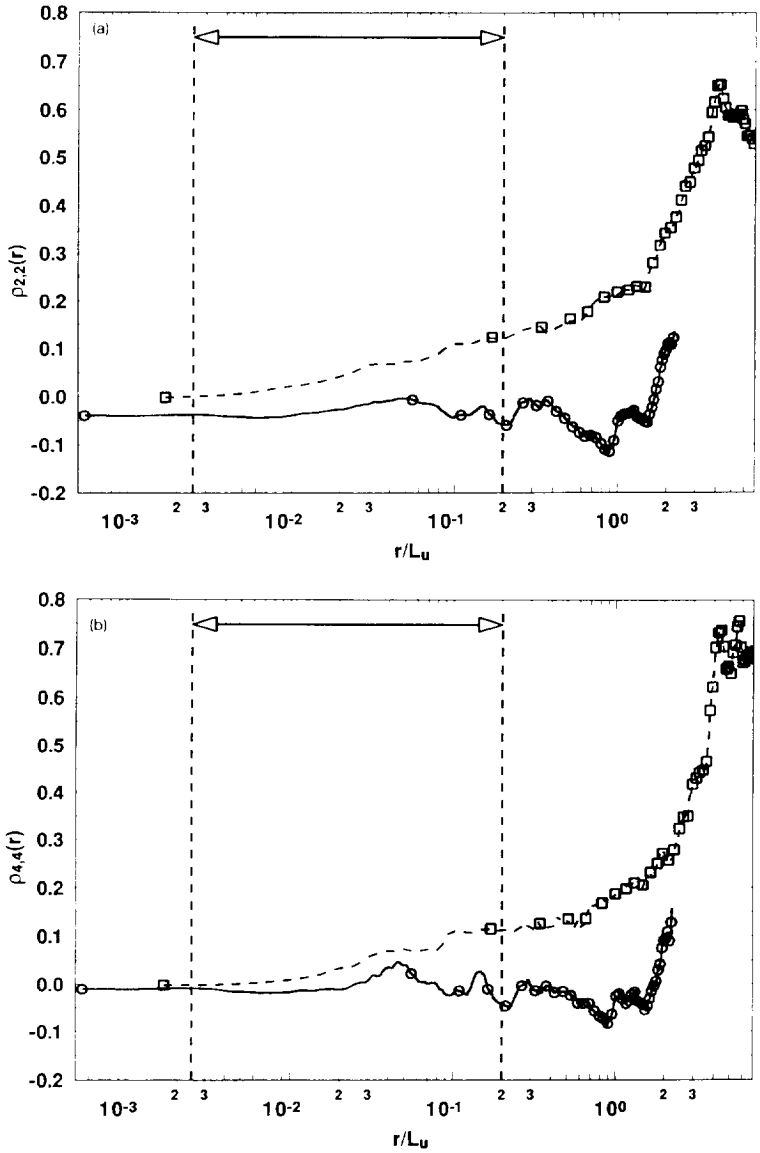

Fig. 7. (a) The evolution of the correlation coefficient $\rho_{m,m}(r)$ as a function of r for $m = 2$ for Runs 1 (open circle) and 2 (open square). The inertial subrange scales are bounded by the two dotted vertical lines. The sweeping decorrelation hypothesis assumes that $\rho_{m,m} = 0$ for all m. (b) Same as (a) but for $m = 4$.

For that purpose, we define the following dimensionless ratio:

$$R_c^{(m)}(r) = \frac{(\rho_{m,m})\,\sigma_{u^m}\,\sigma_{\Delta u^m}}{\langle u_1^m\rangle\langle \Delta u_1^m\rangle}. \tag{23}$$

This ratio is simply the ratio of the first to the second term of the right hand side in (10). That is, R_c measures the ratio of the distortions due to large-scale/inertial-scale interactions to the sweeping

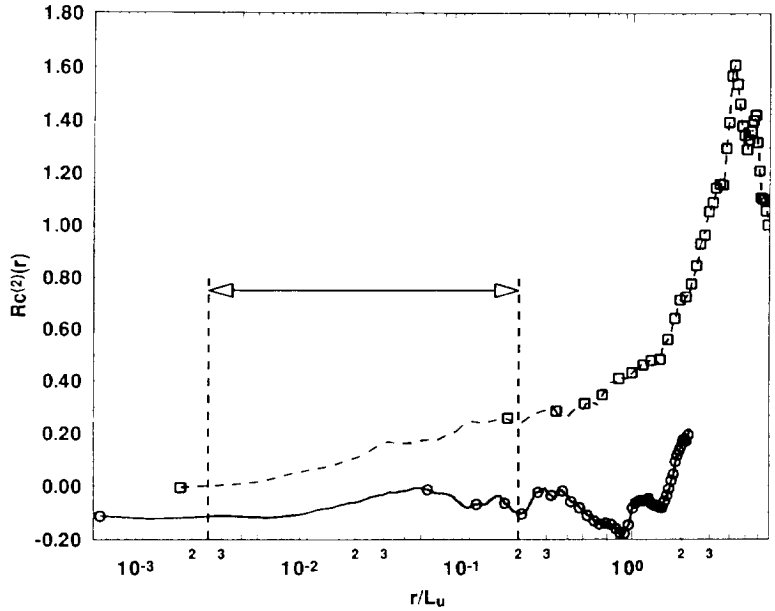

Fig. 8. The evolution of $R_c^{(m)}(r)$ as a function of r for $m = 2$ and Runs 1 (open circle) and 2 (open square). The sweeping decorrelation hypothesis assumes that $R_c(r) = 0$.

motion. For the sweeping decorrelation hypothesis to be valid, this ratio must be negligible. Hence, R_c directly measures the bias in the SDH predictions due to large-scale/inertial-scale interactions (affects the numerator of R_c). In Fig. 8, $R_c(m = 2)$ is shown for Runs 1 and 2. Notice that for Run 2, this ratio increased up to 0.2 indicating partial distortions due to large-scale/inertial subrange interactions at the upper limit of the inertial subrange, which also agrees with Praskovsky et al. (1993) data. The large-scale/inertial subrange interaction suggests that $d^{(m)}(r)$ should be larger than unity for all values of r within subrange, which is not in agreement with the results from Figs. 5a–5c. This motivated us to consider the thermal effects on the local velocity field in the below section.

4.4. Thermal distortions

The above derivation thus far neglected all possible interaction between the velocity and temperature fields within the inertial subrange. We should note here that in the ASL, thermal fluctuations are relatively large even for neutral stratification ($\langle u_3 T \rangle \approx 0$). These temperature disturbances can modify the small scale eddies as they sweep past a Eulerian observer (see e.g. Katul and Parlange, 1994). From previous studies, it is not clear how important these distortions are. One approach for assessing the importance of thermal distortion on the inertial subrange eddy motion is to consider the correlation

$$\rho_{k,l}(r) = \frac{\langle (\Delta T^k - \langle \Delta T^k \rangle)(\Delta u_i^l - \langle \Delta u_i^l \rangle) \rangle}{\sigma_{\Delta T^k} \sigma_{\Delta u^l}}. \tag{24}$$

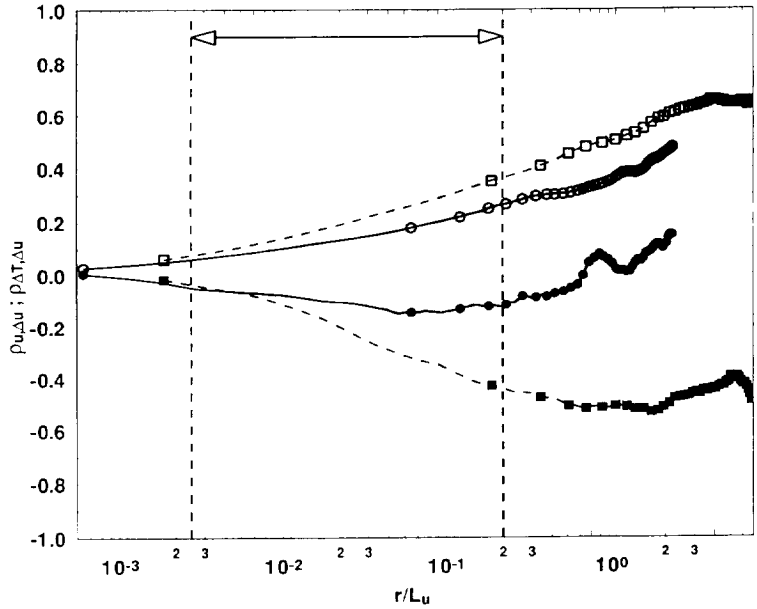

Fig. 9. Comparison between large-scale inertial-scale interaction and local velocity/thermal interaction within the inertial subrange. The evolution of $\rho_{u,\Delta u}(=\langle u_1^1\Delta u_1^1\rangle/[\sigma_{u1}\sigma_{\Delta u1}])$ (open symbols) and $\rho_{\Delta T,\Delta u}(=\langle\Delta T^1\Delta u_1^1\rangle/[\sigma_{\Delta T}\sigma_{\Delta u1}])$ (closed symbols) as a function of r for Runs 1 (circle) and 2 (square). The inertial subrange is also shown. The sweeping decorrelation hypothesis assumes that $\rho_{u,\Delta u}=\rho_{\Delta T,\Delta u}=0$ for all r within the inertial subrange.

where $\Delta T = T(x+r) - T(x)$. If this correlation is significant (for any k and l), then significant distortion of the small-scale eddies occurs due to the temperature fluctuations as they sweep past a Eulerian observer. We also note here that the SDH requires the validity of K41, and central to K41 is the local isotropy assumption. In a locally isotropic velocity field, the velocity differences are uncorrelated with differences of any scalar (see e.g. Monin and Yaglom, 1975). In Fig. 9, we show the dimensionless quantity $\langle\Delta T^1\Delta u_1^1\rangle/(\sigma_{\Delta T1}\sigma_{\Delta u1})$ as a function of r for Runs 1 and 2. For comparison purposes, we also show the dimensionless quantity $\langle u_1^1\Delta u_1^1\rangle/(\sigma_{u1}\sigma_{\Delta u1})$. Recall that the SDH assumes that $\langle u_1^1\Delta u_1^1\rangle = \langle\Delta T^1\Delta u_1^1\rangle = 0$. Notice in Fig. 9 that both correlations are significant. Clearly, some distortions due to large-scale/inertial subrange interaction as well as thermal disturbances exist. However, what is important to note in Fig. 9 is the sign of these correlations. It appears that one distortion mechanism partially counteracts the other distortion mechanism. In essence, the large scale velocity acts to strain the small scale eddies along the horizontal direction while the local thermal disturbances act to distort them in the vertical direction.

5. Conclusions

This study investigated the random sweeping decorrelation hypothesis using the structure function approach. Velocity measurements that exhibit a long inertial subrange, as identified by the third order structure function, were used. These measurements were carried out above a uniform dry lakebed with a uniform fetch exceeding 10 km. It was found that the higher order spectra (up to

$m = 4$) exhibit a well defined $-5/3$ power law. These findings are in agreement with previous atmospheric boundary layer studies over the land and ocean. The sweeping decorrelation hypothesis was examined using two dimensionless quantities that were developed by Praskovsky et al. (1993) to reduce the influence of Taylor's frozen hypothesis. It was found that the sweeping decorrelation hypothesis predictions of the higher-order structure functions overestimated the measurements by 10–30% within the inertial subrange. Although a 10–30% deviation between measurements and predictions may not be large in ASL flows, the direction of this deviation was different from laboratory flows. It was demonstrated that SDH predictions should underestimate the measured higher order structure function, which was contrary to what was measured. Because of this result, two key assumptions, intrinsic to the derivation of the sweeping decorrelation hypothesis, were tested. These assumptions were (i) the absence of large-scale/inertial subrange interaction, and (ii) the absence of any eddy-motion distortions due to thermal disturbances. The latter is usually absent in laboratory experiments. Statistical measures were developed to isolate and investigate these two assumptions. It was found that both of these assumptions were violated in the ASL for neutral and unstable atmospheric conditions. The fact that these two assumptions were violated demonstrate that the SDH cannot be exact for ASL flows. The apparent agreement (10–30%) between the SDH predictions and measurements was attributed to the counteracting nature of these two distortions.

Acknowledgements

The authors would like to thank Scott Tyler for his assistance and support at Owens lake, and Mike Mata and Teresa Ortenburger for aiding in the data collection. We are grateful for the funding support from the National Science Foundation (NSF) grant (EAR-93-04331), United States Geological Survey (USGS), Water Resources Center (WRC) grant (W-812), Kearney Foundation, and UC Davis superfund grant (5 P42ES04699-07).

References

Anselmet, F., Y. Gagne, E.J. Hopfinger and R.A. Antonia (1984) High-order velocity structure functions in turbulent shear flows, *J. Fluid Mech.*, *140*, 63–89.

Chen, S. and R.H. Kraichnan (1989) Sweeping decorrelation in isotropic turbulence, *Phys. Fluids A*, *12*, 2019–2024.

Comte-Bellot, G. and S. Corrsin (1971) Simple Eulerian time correlation of full- and narrow-band velocity signals in grid generated isotropic turbulence, *J. Fluid Mech.*, *48*, 273–337.

Dutton, A.J. and D.G. Deaven (1972) Some observed properties of atmospheric turbulence, in: *Statistical Models and Turbulence, Lecture Notes in Physics* (Springer) 352–383.

Kaimal, J.C. and J.J. Finnigan (1994) *Atmospheric Boundary Layer Flows: Their Structure and Measurement* (Oxford Univeristy Press) pp. 289.

Katul G.G. and M.B. Parlange (1994) On the active role of temperature in surface-layer turbulence, *J. Atmos. Sci.*, *51*, 2181–2195.

Katul, G.G., M.B. Parlange and C.C. Chu (1994a) Intermittency, local isotropy, and non-gaussian statistics in atmospheric surface layer turbulence, *Physics of Fluids*, *6*, 2480–2492.

Katul, G.G., J.D. Albertson, C.C. Chu and M.B. Parlange (1994b) Intermittency in atmospheric surface layer turbulence: The orthonormal wavelet representation, in: *Wavelets in Geophysics*, ed. E. Foufoula and P. Kumar, in press.

Kolmogorov, A.N. (1941) The local structure of turbulence in incompressible viscous fluid for very large Reynolds number, *Dokl. Akad. Nauk. SSSR*, 30, 301–303.

Kuznetsov, V.R., A. Praskovsky and V.A. Sabelnikov (1992) Fine-scale turbulence structure of intermittent shear flows, *J. Fluid Mech.*, *243*, 595–622.

Landau, L.D. and E.M. Lifshitz (1987) *Fluid Mechanics* (Pergamon) pp. 140, 539.

McComb, W.D., V. Shanmugasundaram and P. Hutchinson (1989) Velocity derivative skewness and two-time velocity correlations of isotropic turbulence as predicted by LET theory, *J. Fluid Mech.*, *208*, 91.

McComb, W.D. (1991) *The Physics of Fluid Turbulence* (Oxford Science Publications) pp. 144, 572.

Monin, A.S. and A.M. Yaglom (1975) *Statistical Fluid Mechanics* (MIT Press) Ch. 8, pp. 401, 875.

Nelkin, M. and M. Tabor (1990) Time correlations and random sweeping in isotropic turbulence, *Phys. Fluids A*, *2*, 81–83.

Praskovsky, A.A., E.B. Gledzer, M.Y. Karyakin and Y. Zhou (1993) The sweeping decorrelation hypothesis and energy-inertial scale interaction in high Reynolds number flows, *J. Fluid Mech.*, *248*, 493–511.

Sanada, T., and V. Shanmugasundaram (1992) Random sweeping effect in isotropic numerical turbulence, *Phys. Fluids A*, *4*, 1245–1250.

Shlien, D.J. and S. Corrsin (1974) A measurement of lagrangian velocity autocorrelation in approximately isotropic turbulence, *J. Fluid Mech.*, *62*, 255–271.

Sirivat, A. and Z. Warhaft (1983) The effect of a passive cross-stream temperature gradient on the evolution of temperature variance and heat flux in grid turbulence, *J. Fluid Mech.*, *128*, 323–346.

Taylor, G.I. (1938) The spectrum of turbulence, *Proc. Roy. Soc., A. Vol. CLXIV*, 476–490.

Tennekes, H. (1975) Eulerian and Lagrangian time microscales in isotropic turbulence, *J. Fluid Mech.*, *67*, 561–567.

Van Atta, C.W. and J.C. Wyngaard (1975) On higher-order spectra of turbulence, *J. Fluid Mech.*, *72*, 673–694.

Wyngaard, J.C. and Y.H. Pao (1972) Some measurements of the fine structure of large Reynolds number turbulence, in: *Statistical Models and Turbulence, Lecture Notes in Physics* (Springer) pp. 384–401, 492.

Wyngaard, J.C. (1981) Cup, propeller, vane, and sonic anemometer in turbulence research, *Ann. Rev. Fluid Mech.*, *13*, 922–929.

Yakhot, V., S.A. Orszag and Z.S. She (1989) Space-time correlations in turbulence: kinematical versus dynamical effects, *Phys. Fluids A 2*, 184–186.